Int. J. Heat Mass Transfer. Vol. 33, No. 10, pp. 2285–2293, 1990
Printed in Great Britain

0017-9310/90 $3.00 + 0.00

Experiments on subcooled flow boiling heat transfer in a vertical annular channel

A. HASAN and R. P. ROY
Department of Mechanical and Aerospace Engineering, Arizona State University, Tempe, AZ 85287, U.S.A.

and

S. P. KALRA
Nuclear Power Division, Electric Power Research Institute, Palo Alto, CA 94303, U.S.A.

(*Received* 31 *May* 1989 *and in final form* 27 *December* 1989)

Abstract—Experiments on subcooled flow boiling heat transfer are carried out in a vertical annular channel the inner wall of which is heated and the outer wall insulated. Refrigerant-113 is the working fluid. Flow boiling heat transfer data are reported at three mass velocities (579, 801, and 1102 kg m^{-2} s^{-1}), three pressures (312, 277, and 243 kPa), and three inlet subcoolings (20.0, 30.0, and 36.5°C). A multiple-hysteresis phenomenon is identified. The measured wall heat transfer coefficients are compared with predictions by various correlations and an improvement of the Shah correlation for annuli is suggested.

INTRODUCTION

NUCLEATE boiling is an important mechanism of heat transfer from a surface to fluid flowing adjacent to it. The fluid may be either subcooled or saturated at the prevalent pressure. Because of its efficient heat transfer characteristics, nucleate flow boiling has been the subject of numerous investigations, some emphasizing experiments (e.g. refs. [1–5]) and others concentrating on examination and analysis of data reported in the literature to develop predictive correlations for the heat transfer rate from the surface (e.g. refs. [6–11]). Experiments such as refs. [1, 4, 5] and empirical analyses such as refs. [6, 7, 9–11] have dealt specifically with subcooled flow boiling. An empirical correlation developed by Chen [8], although originally meant for saturated flow boiling conditions, was extended later by others to the subcooled boiling situation [12].

In this paper, we report heat transfer measurements in subcooled nucleate boiling flow of Refrigerant-113 (R-113) through a vertical annular channel the inner wall of which is heated and the outer wall insulated. The measured variables are: the inner wall heat flux and temperature, radial distribution of the liquid phase temperature, mass velocity of the fluid, local pressure at the measurement plane, and the dissolved air content of R-113 (so that the partial pressure of R-113 and thus its true saturation temperature can be determined). Boiling curves are presented as are plots of the measured wall heat transfer coefficient. The wall heat transfer coefficient is defined here as

$$h = \frac{q''_w}{(\bar{T}_w - \bar{T}_{bl})}. \quad (1)$$

The rationale for our use of $\bar{T}_{bl}$ in place of the more common $\bar{T}_{b,fluid}$ is two-fold: $\bar{T}_{bl}$ is a state variable which appears naturally in two-fluid models of boiling flow, and it is also the temperature at which the liquid phase properties are calculated in various wall heat transfer coefficient correlations. The use of $\bar{T}_{b,fluid}$ calculated from the heat balance consideration would be an equally appropriate alternative in the presentation of the wall heat transfer coefficient data.† The measured values of h are compared with predictions by Shah [9], modified Shah,‡ Gungor–Winterton [11], and Chen [8, 12] correlations. The Shah correlation pertains specifically to subcooled boiling flow of fluids in annuli. An earlier paper by us [13] contains additional information regarding the single-phase liquid heat transfer coefficient data which appears in the plots presented here. The effect of natural convection in the experiments reported here can be considered to be negligible because even at the lowest mass velocity the parameter (Grashof number)/(Reynolds number)^2 is much smaller than unity.

EXPERIMENTAL APPARATUS

The experimental rig has been described in an earlier paper [14] and as such, only the annular test section will be described here. The outer segment of the test section consisted of two long pieces of transparent

† This is discussed further in a later section of the paper.
‡ The modification involves the single-phase liquid forced convection portion of the correlation and is explained in a later section.

NOMENCLATURE

A_{x-s}	flow area of test section	$\bar{T}_{bl}$	time-averaged mixed-mean temperature of the liquid phase
Bo	boiling number	$\bar{T}_l$	time-averaged local temperature of the liquid phase
D_h	hydraulic diameter of annulus, $2(r_{outer}-r_{inner})$	$T_{sat,r}$	saturation temperature of R-113 at its partial pressure
h	wall heat transfer coefficient	$\bar{T}_w$	time-averaged temperature of the heated wall
p	pressure	$\Delta T_{sub,in}$	liquid subcooling at test section inlet
p_r	partial pressure of R-113	$\bar{u}_l$	time-averaged axial velocity of liquid
q''_w	wall heat flux	X_{tt}	Martinelli parameter.
r	radial coordinate		
Re_l	liquid Reynolds number		
$\bar{T}_{b,fluid}$	time-averaged mixed-mean temperature of the fluid		

Pyrex glass pipe (38.6 mm i.d., 47.0 mm o.d.) with a 0.5 m long 304 stainless steel section of the same i.d. in between them. The stainless steel section will henceforth be referred to as the 'measurement section'. A 304 stainless steel tube, of 15.9 mm o.d. and 1.2 mm wall thickness, constituted the inner segment of the test section. The total length of the test section was 3.66 m of which the upper 2.75 m could be heated via resistive heating of the inner tube (d.c., 38 kW maximum heating power). The measurement plane (in the measurement section) was approximately 86 hydraulic diameters downstream of the beginning of the heated length. Concentricity of the test section was maintained by means of four support vane assemblies, each assembly consisting of four 9 mm long and 1 mm thick vanes arranged in a $\times$-configuration, carefully welded to the inner tube at equal axial spacings. The nearest vane assembly upstream of the measurement plane was about 32 hydraulic diameters away. The heater tube was filled with aluminium oxide powder for insulation. The outer segment of the test section was insulated with 50 mm thick jacketed fiber glass wool.

Figure 1 shows, schematically, the locations of two hot-film sensors and two (out of a total of four) wall thermocouples in the measurement section. The fluid temperature measurements were performed by the two hot-film sensors, TSI models 1262AE-10W (a miniature cylindrical sensor, 25 μm diameter and 51 μm long) and 1264-BP (a miniature conical probe, 30° tip angle, with the sensor film located very close to the tip), located diametrically opposite each other. Although the hot-film probes were intrusive, they were designed (via miniaturization and 90° bend) to minimize the resulting disturbance to the measurement plane flow field. Each sensor was operated with a constant-current module (TSI 1040). The slight difference in the fluid temperature due to the axial separation of about 3 mm between the sensors was estimated and found to be well within the experimental uncertainty.

The heated wall temperature at approximately the same axial location as the hot-film sensors (see Fig. 1) was measured by means of two copper–constantan surface thermocouples (STC; Omega, foil-thickness $\simeq$0.012 mm) baked on with Omegabond epoxy to the heater tube inner wall. The tube inner wall temperature was read off a multichannel temperature monitor (Omega 2176A-T). The heater tube outer wall (which is the heated wall of the annulus) temperature was then calculated by a steady state heat conduction analysis. The wall temperature data presented in this paper are from STC #1. The discrepancy in the value of the mixed-mean liquid phase (or fluid) temperature due to the slight mismatch between the surface thermocouple location and the hot-film sensor locations was estimated to be less than 0.1°C.

The volumetric flow rate of liquid at the test section inlet was measured by means of a turbine flow meter (Flow Technology, Model FT-12). The pressure at the measurement plane was measured by means of an accurate pressure gauge (Omega, Model PGT-45L-60).

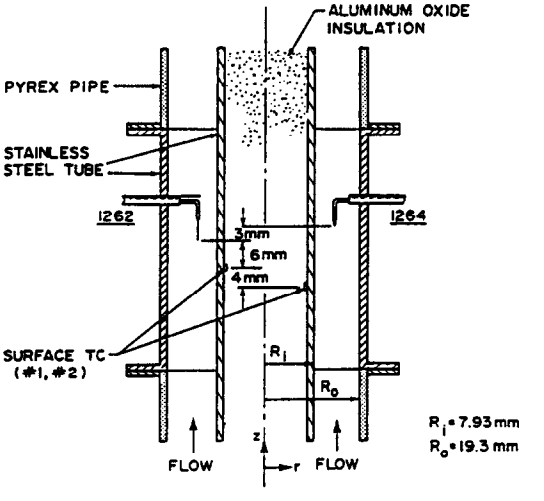

FIG. 1. The annular test section.

A dedicated system (DATA 6000A, Analogic) with floppy disk drive and plotter peripherals was used to acquire, store, analyze and display the time series data for fluid temperature.

EXPERIMENTAL PROCEDURE

Temperature calibration

The hot-film sensors and the wall thermocouples were calibrated *in situ* by increasing the temperature of liquid R-113 entering the test section in stages by means of a preheater located upstream. The test section itself was unheated.

Dissolved air content of R-113

It is well known that R-113 quickly absorbs air from the surrounding atmosphere. The dissolved air lowers the partial pressure of R-113 at any given temperature, thereby significantly affecting the boiling process. For example, the onset of nucleate boiling at a heated surface is expedited.

The dissolved air content of R-113 was measured by bleeding off fluid from the experimental rig and then using an aireometer (Seaton–Wilson AD-4003). The same procedure had been used by Murphy and Bergles [4]. The partial pressure of air in the solution was found by applying Henry's law along with the value of K_{air} provided by DuPont (Bulletin B-14B, 1967). The R-113 partial pressure was then equal to the total pressure minus the air partial pressure. The true saturation temperature of R-113, $T_{sat,r}$, corresponds to the partial pressure of R-113.

The experiments

The nucleate flow boiling heat transfer experiments were carried out in two different modes: one mode in which the wall heat flux was gradually increased from a low initial value at which single-phase liquid forced convection existed, and another in which the wall heat flux was gradually decreased from a high initial value at which fully-developed subcooled nucleate boiling prevailed. The majority of the experiments were conducted in the increasing heat flux mode although several series of experiments were repeated in the decreasing heat flux mode. In the latter, the wall heat flux was lowered through the same set of values as in the corresponding increasing-heat flux mode experiments, the intent being to examine the hysteresis effect in flow boiling.

For each experiment series (as defined by the fluid mass velocity, pressure and subcooling at the test section inlet) a set of wall heat flux values was selected such that the range from single-phase liquid forced convection to fully-developed nucleate boiling would be spanned. At each heat flux a steady state was established. The wall temperature was then measured by STC #1 and STC #2. The hot-film sensors were manually traversed in the radial direction and at each location a temperature signal time series was recorded in the data acquisition system. In the event of the sensors being in the two-phase fluid region, a probability density function (PDF, or histogram) was constructed from the signal time series to determine if the sensor was fast enough to recognize both the liquid phase and the vapor phase temperatures.† The PDFs obtained from the miniature conical probe indicated that this probe was too sluggish to respond to the passage of discrete vapor bubbles (the bubbles were often of the order of 1 mm or smaller) and essentially measured the liquid temperature distribution. Having thus measured the liquid phase temperature radial distribution and assuming an appropriate axial velocity profile for the liquid (this profile should be somewhat flatter than the turbulent axial velocity profile for single-phase liquid flow through the annulus [16]), the mixed-mean temperature of the liquid phase was calculated as

$$\bar{T}_{bl} = \frac{\int_{A_{x-s}} \bar{u}_l(r)\bar{T}_l(r)\,dA}{\int_{A_{x-s}} \bar{u}_l(r)\,dA}. \quad (2)$$

This temperature was then used in the calculation of the wall heat transfer coefficient by equation (1).

Our method of comparison of the measured wall heat transfer coefficient with the predictions of various subcooled flow boiling correlations for the same coefficient is tantamount to comparing the measured heated wall temperature to the predicted ones at the prevalent fluid condition. The wall heat transfer coefficient can be predicted by using the differential between the wall temperature calculated from a certain correlation and either $\bar{T}_{bl}$, obtained in accordance with equation (2), or $\bar{T}_{b,fluid}$, the mixed-mean fluid temperature obtained from a heat balance.‡ The same mixed-mean temperature must then be used to obtain the measured heat transfer coefficient. Thus, uncertainty in the assumed liquid phase velocity profile in equation (2) does not affect the validity of the comparisons presented in the next section.

RESULTS

Table 1 shows the ranges of variables over which the experiments were conducted and the associated measurement uncertainties.

Flow boiling curves

Figures 2 and 3 show single-phase liquid forced convection and subcooled nucleate boiling heat trans-

† The vapor phase temperature can, of course, be expected to be narrowly distributed around the local R-113 saturation temperature with a peak at the saturation temperature [15].

‡ The preferred option will depend upon the details of the model that one wishes to use for describing subcooled boiling flow. As mentioned earlier, the mixed-mean liquid phase temperature appears naturally in two-fluid models and hence may be preferred.

Table 1. Ranges of experiments and measurement uncertainties

	Range	Uncertainty
Heat flux	1×10^4–1.5×10^5 W m^{-2}	±80 W m^{-2}
Wall temperature	60–100°C	±0.4°C
Wall heat transfer coefficient	400–6000 W m^{-2} K^{-1}	±5%
Mass velocity	579–1102 kg m^{-2} s^{-1}	±3 kg m^{-2} s^{-1}
Pressure at measurement plane	243–312 kPa	±0.7 kPa
Subcooling at test section inlet	20–37°C	±0.1°C
Time-averaged local liquid phase temperature (at measurement plane)	45–72°C	±0.2°C
Sensor radial traverse (in annulus)	0–10 mm	±30 μm

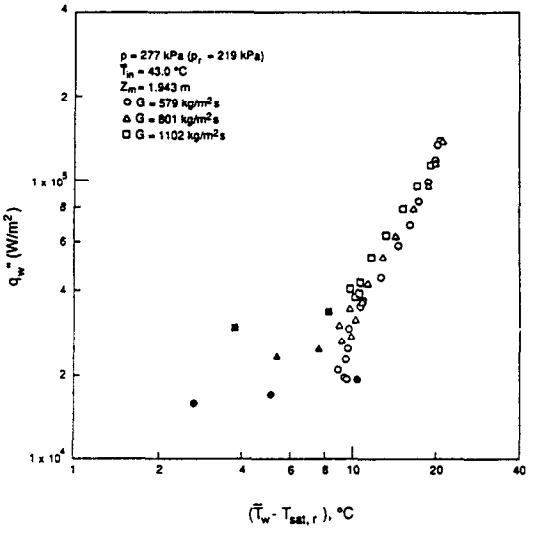

FIG. 2. Flow boiling curves at three mass velocities (the filled symbols indicate single-phase liquid data).

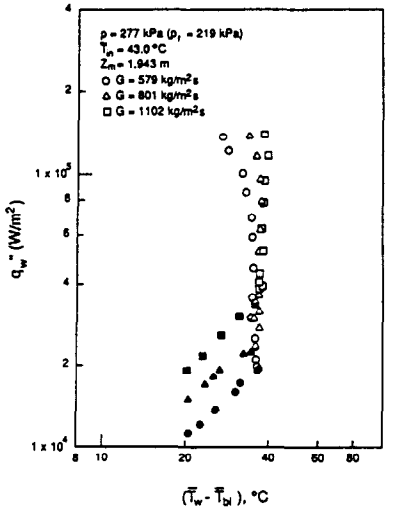

FIG. 3. Wall heat flux vs the difference between wall and mixed-mean liquid phase temperatures at three mass velocities.

fer data at three mass velocities (579, 801, and 1102 kg m^{-2} s^{-1}) at a measurement plane pressure of 277 kPa (this corresponded to R-113 partial pressure of 219 kPa at the prevalent dissolved air content) and a liquid temperature at the test section inlet of 43.0°C (subcooling of 30.0°C). The data shown pertain to the increasing-heat flux mode. In Fig. 2, the wall heat flux has been plotted vs the wall superheat (defined as $\bar{T}_w - T_{sat,r}$), whereas in Fig. 3 the wall heat flux is plotted vs the temperature difference between the wall and the mixed-mean liquid, $\bar{T}_w - \bar{T}_{bl}$. The phenomenon of delayed nucleation followed by a sudden drop in the wall temperature (hysteresis), typical of 'wetting liquid–commercially prepared surface' combinations, is apparent as is the trend of decrease in the magnitude of hysteresis with increase in mass velocity. These trends are in agreement with the observations of Murphy and Bergles [4]. A region of partial nucleate boiling can be observed immediately after the hysteresis region followed by an asymptotic approach to the fully-developed nucleate boiling mode. The fully-developed mode is essentially insensitive to variations in the mass velocity. All of these features are consistent with the findings of earlier investigators (e.g. refs. [1, 4]).

Figure 4 shows two boiling curves at a mass velocity of 579 kg m^{-2} s^{-1}, pressure of 277 kPa, and inlet liquid temperature of 43.0°C where wall temperatures measured by STC #1 and #2 are plotted to demonstrate typical data scatter. Except in the vicinity of hysteresis, the temperatures measured by the surface thermocouples are within ±0.4°C of each other. The difference in the extent of hysteresis in the two curves may be explained by small variations in local surface condition (e.g. finish).

Figures 5 and 6 show single-phase liquid forced convection and subcooled nucleate boiling heat transfer data at three measurement plane pressures, namely 312, 277, and 243 kPa (these correspond to R-113 partial pressures of 253, 219, and 184 kPa, respectively). It is evident from Fig. 6 that pressure has essentially no influence on single-phase liquid forced convection heat transfer, the changes in the physical properties of the liquid with pressure being negligible. In Fig. 5, a larger hysteresis effect can be deciphered at lower pressure. Figure 5 also shows that as the pressure increases the wall superheat decreases at the

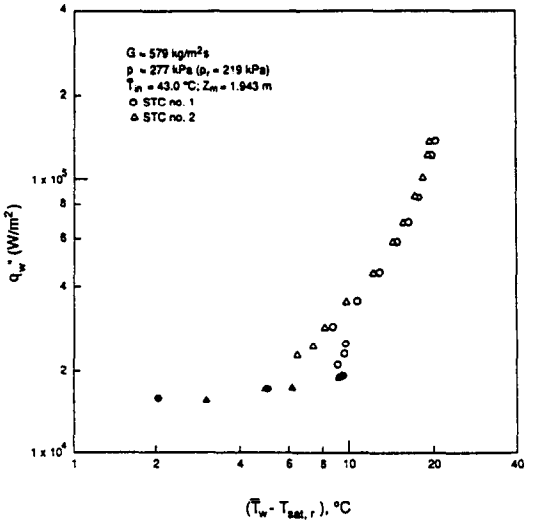

FIG. 4. Flow boiling curve data scatter due to two wall thermocouples at diametrically opposite locations.

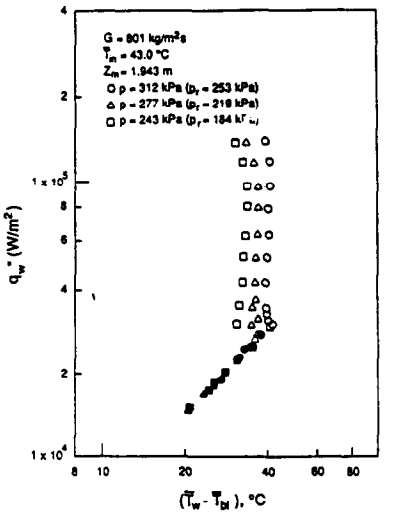

FIG. 6. Wall heat flux vs the difference between wall and mixed-mean liquid phase temperatures at three pressures.

same wall heat flux. This effect in the nucleate boiling region was also reported by Hsu and Graham [17] who ascribed it to the variations in the specific volume difference between the vapor and liquid phases as well as surface tension. Figure 6, on the other hand, shows that as pressure increased, $\bar{T}_w - \bar{T}_{bl}$ increases in the nucleate boiling region at the same wall heat flux.

Figures 7 and 8 show single-phase liquid forced convection and subcooled nucleate boiling heat transfer data at three different inlet subcoolings, namely 20.0, 30.0, and 36.5°C, at a measurement plane pressure of 277 kPa and mass velocity of 801 kg m^{-2} s^{-1}. In the single-phase liquid region, a larger heat flux can be sustained at the same wall superheat as the local liquid subcooling increases which, of course, is expected. The heat transfer coefficient as given by equation (1) remains essentially constant here (Fig. 8). It is evident from Fig. 7 that the wall superheat remains lower at higher subcoolings in the partial boiling region followed by an asymptotic approach to fully-developed boiling where the influence of subcooling becomes minimal. Figure 8 shows that the temperature difference between the wall and the mixed-mean liquid phase is lower at lower subcoolings at any given heat flux in both the partial and fully-developed boiling regions resulting in higher heat transfer coefficients at lower subcoolings.

It was noted by earlier investigators (e.g. refs. [1, 4]) that the boiling curve data in the nucleate boiling region for the decreasing-heat flux experiments follow those of the increasing-heat flux experiments until the hysteresis region is approached. Figure 9 shows this

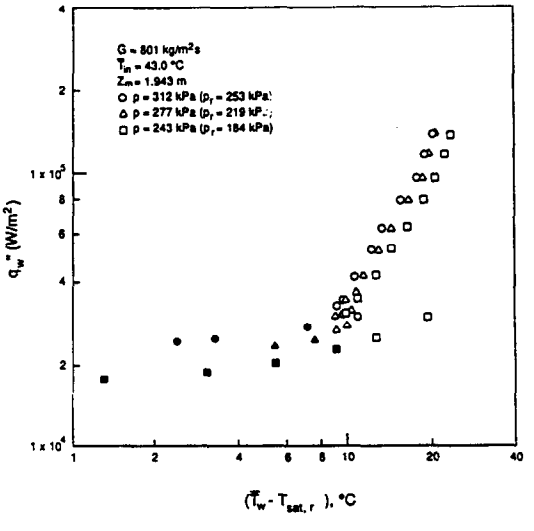

FIG. 5. Flow boiling curves at three different pressures.

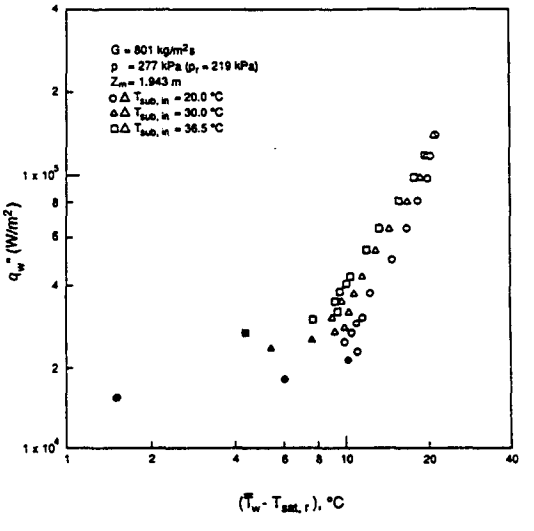

FIG. 7. Flow boiling curves at three different subcoolings.

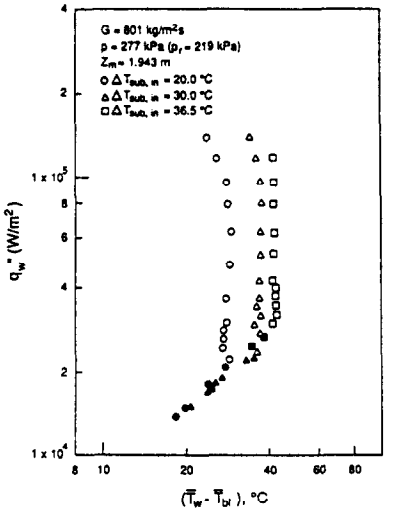

FIG. 8. Wall heat flux vs the difference between wall and mixed-mean liquid phase temperatures at three subcoolings.

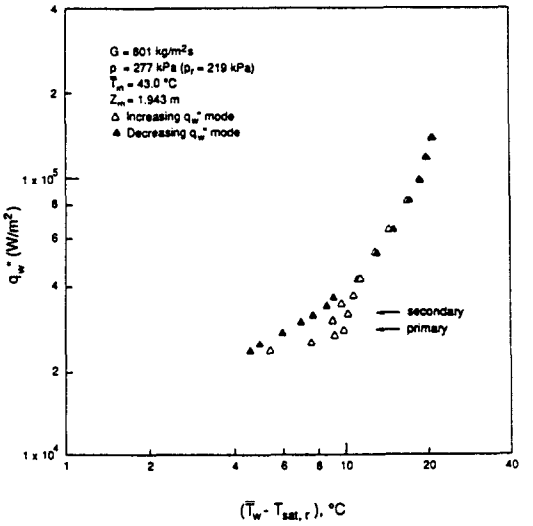

FIG. 9. Multiple-hysteresis effect.

behavior at a mass velocity of 801 kg m^{-2} s^{-1}, measurement plane pressure of 277 kPa and inlet liquid temperature of 43.0°C. Additional experiments run at other mass velocity–pressure–inlet temperature combinations exhibit similar behavior.

One other feature of the data in the hysteresis region is noteworthy. This pertains to the appearance, in some instances, of a multiple-hysteresis (primary, secondary, etc.) pattern with gradually diminishing amplitude as the wall heat flux is increased. Such a pattern can be recognized in the data of Fig. 9. The multiple-hysteresis phenomenon in a wetting liquid–commercially prepared surface combination may be explained as a sequence of superheat buildups followed by sudden temperature drops upon activation of cavities which continue well into the partial boiling region albeit with decreasing amplitude.

Wall heat transfer coefficient

The definition of wall heat transfer coefficient given by equation (1) pertains to both single-phase liquid flow and boiling flow in this work. In ref. [13], we presented the single-phase liquid turbulent flow data and compared them to four different correlations/analyses, namely, Dittus–Boelter, Colburn, Kays–Leung, and Gnielinski.

Figure 10 shows plots of the wall heat transfer coefficient vs the heat flux at three mass velocities. Both single-phase liquid and flow boiling data are included. Also shown for comparison are predictions of wall heat transfer coefficient by the Shah correlation [9].† The Shah correlation reduces to the Dittus–Boelter correlation in the event of single-phase liquid flow.

It is immediately noticeable in Fig. 10 that the single-phase liquid data do not compare very well with the Dittus–Boelter correlation. Our own best fit for the annular test section in the Reynolds number range of 20 000–50 000 is [13]

$$Nu = 0.0106 Re^{0.88} Pr^{0.4}. \quad (3)$$

If equation (3) is used in the Shah correlation in place of the Dittus–Boelter correlation, the agreement

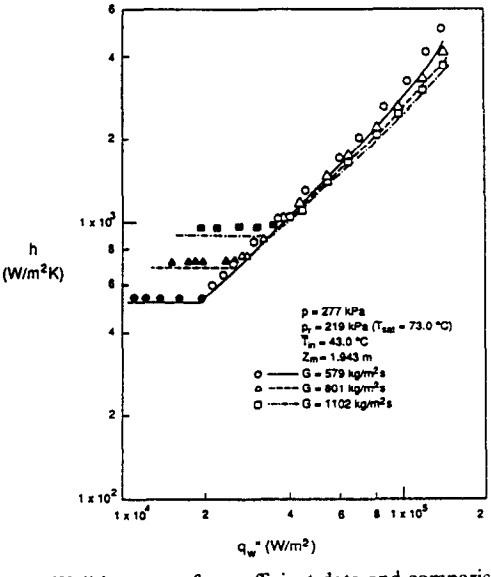

FIG. 10. Wall heat transfer coefficient data and comparison with the Shah correlation.

† A distinction is made between 'high subcooling' and 'low subcooling' condition in the Shah correlation. In the majority of our experiments the 'low subcooling' condition existed at the measurement plane and the corresponding correlation was used in predicting the wall heat transfer coefficient. There were a few low heat flux experiments where the 'high subcooling' condition existed. Even in these cases, however, the 'low subcooling' correlation gave better agreement with our data and was, therefore, used.

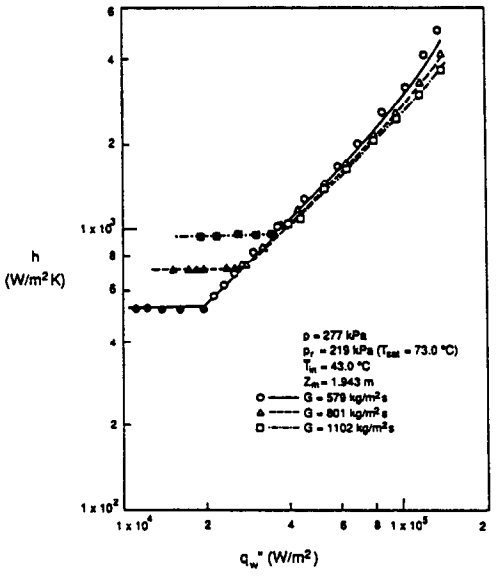

FIG. 11. Wall heat transfer coefficient data and comparison with the modified Shah correlation.

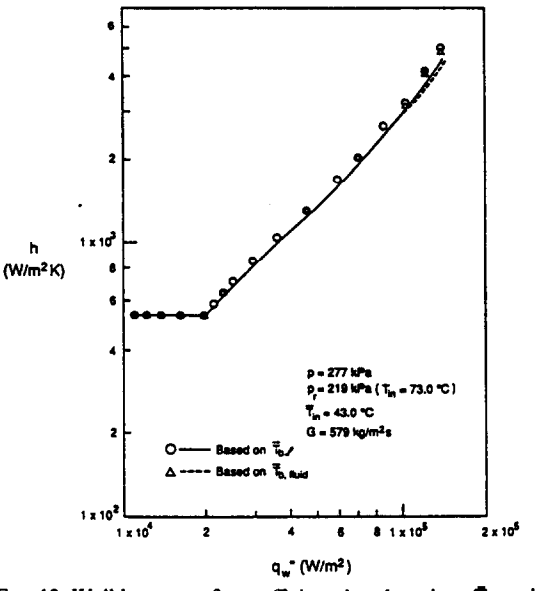

FIG. 12. Wall heat transfer coefficient data based on $\bar{T}_{bl}$ and $\bar{T}_{b,fluid}$ and comparison with the modified Shah correlation.

between the heat transfer coefficient predictions and measured data is much better in the subcooled nucleate boiling region as seen in Fig. 11. This modification is henceforth referred to as the 'modified Shah correlation'.

We studied the use of the Gnielinski correlation for single-phase forced convection in an annular geometry [18] in place of the Dittus–Boelter correlation in the original correlation of Shah. This also resulted in better agreement between the measurements and predictions in the single-phase liquid and subcooled nucleate boiling regions although the improvement was not as consistent as when equation (3) was used. Nevertheless, this demonstrates that the accuracy of subcooled nucleate boiling wall heat transfer coefficient correlations depends rather strongly on the proper choice of the single-phase liquid forced convection heat transfer correlation.

In Figs. 10 and 11, the data as well as the correlations point to a trend of decreasing wall heat transfer coefficient with increase in mass velocity in the subcooled boiling region. This is especially the case at higher heat fluxes as fully-developed subcooled boiling occurs. The trend can be explained as follows: in fully-developed subcooled flow boiling, the wall temperature is essentially independent of mass velocity [6, 7]. However, as the mass velocity increases at the given wall heat flux, the mixed-mean liquid (or fluid) temperature decreases. Thus, the wall heat transfer coefficient decreases with increase in mass velocity.

Figure 12 shows plots of the wall heat transfer coefficient, h, calculated as

$$\frac{q''_w}{(\bar{T}_w - \bar{T}_{bl})} \quad \text{and} \quad \frac{q''_w}{(\bar{T}_w - \bar{T}_{b,fluid})}$$

vs wall heat flux at the mass velocity of 579 kg m^{-2} s^{-1}. As explained earlier, any change in the value of h due to the use of $\bar{T}_{b,fluid}$ in place of $\bar{T}_{bl}$ would be of the same magnitude for the measured data and the predicted correlation. This is apparent from the figure.

Figure 13 shows a comparison of the measured wall heat transfer coefficients at three pressures with the modified Shah correlation. Again, the agreement is quite good. While essentially no influence of pressure is seen on the single-phase liquid coefficient, the heat transfer coefficient in the subcooled nucleate boiling

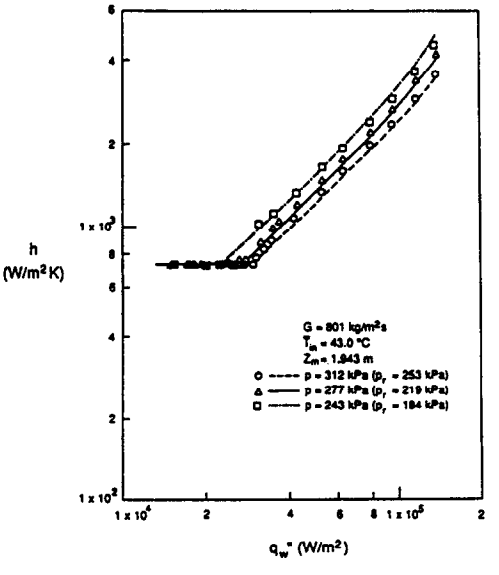

FIG. 13. Wall heat transfer coefficient data and comparison with the modified Shah correlation.

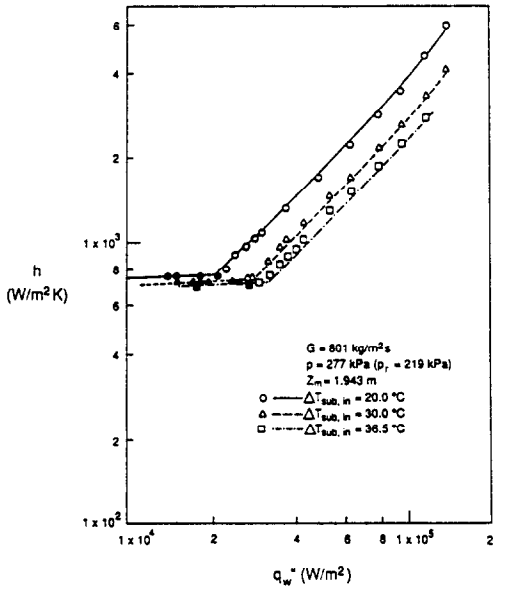

FIG. 14. Wall heat transfer coefficient data and comparison with the modified Shah correlation.

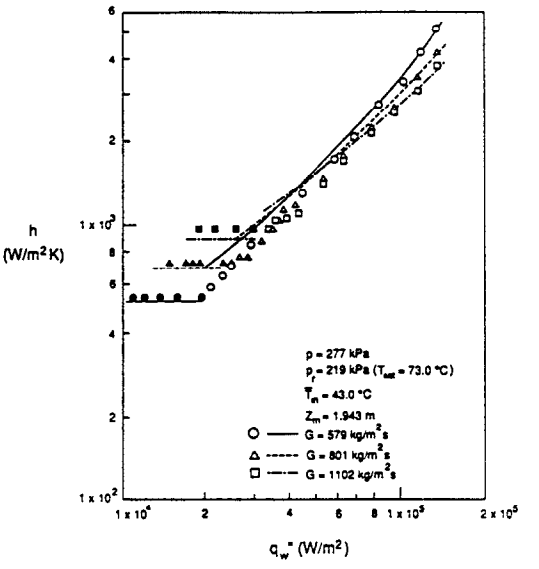

FIG. 15. Wall heat transfer coefficient data and comparison with the Gungor–Winterton correlation.

region decreases with increase in pressure. A possible explanation is as follows.

The temperature difference between the wall and the bulk (mixed-mean) liquid can be expressed as

$$\bar{T}_w - \bar{T}_{bl} = (\bar{T}_w - T_{sat,r}) + (T_{sat,r} - \bar{T}_{bl}). \quad (4)$$

While the saturation temperature increases with increasing pressure, the difference between the wall temperature and the saturation temperature decreases because of an increase in the density of nucleation sites caused mainly by a reduction in the surface tension of the fluid. At the same time however, the difference between the saturation temperature and the bulk liquid temperature increases by a sufficient enough magnitude to more than compensate for the decrease in $(\bar{T}_w - T_{sat,r})$. The end effect is that $(\bar{T}_w - \bar{T}_{bl})$ increases with increasing pressure which translates to a decrease in the wall heat transfer coefficient.

Figure 14 shows a comparison of the heat transfer coefficient data at three inlet liquid subcoolings with the modified Shah correlation predictions. The agreement is good. A trend of decreasing wall heat transfer coefficient in the nucleate boiling region can be identified as the subcooling is increased. Again, the essentially invariant wall temperature at any given pressure explains this trend.

A correlation for the wall heat transfer coefficient at saturated flow boiling in tubes and annuli has been developed by Gungor and Winterton [11]. For subcooled flow boiling they suggest a modification which involves setting the 'enhancement factor, E' in their correlation to unity but retaining the 'suppression factor, S'. Figure 15 shows a comparison of the wall heat transfer coefficient data with values predicted by this correlation in which the suppression factor is calculated from the expression.

$$S = \frac{1}{1 + 1.15 \times 10^{-6} E^2 \, Re_l^{1.17}} \quad (5)$$

after setting E to unity. If, however we use the value of E obtained from their suggested expression

$$E = 1 + 24\,000 Bo^{1.16} + 1.37(1/X_{tt})^{0.86} \quad (6)$$

in calculating S (this may be one interpretation of how this correlation should be used), the agreement between our data and the correlation becomes poor.

It is apparent from Fig. 15 that the agreement between our data and the Gungor–Winterton subcooled boiling correlation improves as the degree of subcooling decreases. In the highly subcooled region however, the agreement is not as good as it is with the modified Shah correlation.

The wall heat transfer coefficient data were also compared with the Chen correlation as modified for use in subcooled flow boiling situations [8, 12]. The agreement was generally poor.

CONCLUDING REMARKS

The experiments reported here confirm the effects of mass velocity, pressure, and subcooling on partial and fully-developed subcooled nucleate flow boiling heat transfer. The Shah correlation when modified by replacing the Dittus–Boelter correlation for single-phase liquid convective heat transfer by one better suited to the annular geometry is able to predict the wall heat transfer coefficient quite well.

Acknowledgements—This work was supported by Electric Power Research Institute, Nuclear Power Division, under research project RP 2398.

REFERENCES

1. A. E. Bergles and W. M. Rohsenow, The determination of forced convection surface boiling heat transfer, *ASME J. Heat Transfer* **86**, 365–372 (1964).
2. V. E. Schrock and L. M. Grossman, Forced convection boiling in tubes, *Nucl. Sci. Engng* **12**, 474–480 (1962).
3. F. Kreith and M. Summerfield, Heat transfer to water at high flux densities with and without surface boiling, *Trans. ASME* **71**(7), 805–815 (1949).
4. R. W. Murphy and A. E. Bergles, Subcooled flow boiling of fluorocarbons, DSR 71340 and 71903, Massachusetts Institute of Technology (1971).
5. H. Müller-Steinhagen, A. P. Watkinson and N. Epstein, Subcooled boiling and convective heat transfer to heptane flowing in an annulus and past a coiled wire: Part I—experimental results, *ASME J. Heat Transfer* **108**, 922–928 (1986).
6. W. H. Jens and P. A. Lottes, Analysis of heat transfer, burnout, pressure drop and density data for high pressure water, ANL-4627 (1951).
7. J. R. S. Thom, W. M. Walker, T. A. Fallon and G. F. S. Reising, Boiling in subcooled water during flow up heated tubes or annuli, *Proc. Instn Mech. Engrs* **180**, 226 (1965).
8. J. C. Chen, Correlation for boiling heat transfer to saturated fluids in convective flow, *I & EC Process Des. Dev.* **5**, 323 (1966).
9. M. M. Shah, Generalized prediction of heat transfer during subcooled boiling in annuli, *Heat Transfer Engng* **4**(1), 24–31 (1983).
10. H. Müller-Steinhagen, A. P. Watkinson and N. Epstein, Subcooled boiling and convective heat transfer to heptane flowing inside an annulus and past a coiled wire: Part II—correlation of data, *ASME J. Heat Transfer* **108**, 928–933 (1986).
11. K. E. Gungor and R. H. S. Winterton, A general correlation for flow boiling in tubes and annuli, *Int. J. Heat Mass Transfer* **29**, 351–358 (1986).
12. J. G. Collier, *Convective Boiling and Condensation*. McGraw-Hill, New York (1981).
13. A. Hasan, R. P. Roy and S. P. Kalra, Heat transfer measurements in turbulent liquid flow through a vertical annular channel, *ASME J. Heat Transfer* **112**(1), 247–250 (1990).
14. R. P. Roy, P. Jain and S. P. Kalra, Dynamic instability experiments in a boiling flow system, *Int. J. Heat Mass Transfer* **31**, 1947–1952 (1988).
15. J. M. Delhaye, R. Semeria and J. C. Flamand, Void fraction, vapor and liquid temperatures; local measurements in two phase flow using a microthermocouple, *ASME J. Heat Transfer* **95**, 363–370 (1973).
16. R. P. Roy, V. S. Krishnan and A. Raman, Measurement in turbulent liquid flow through a vertical concentric annular channel, *ASME J. Heat Transfer* **108**(1), 199–202 (1986).
17. Y. Y. Hsu and R. W. Graham, *Transport Process in Boiling and Two-phase Systems*. Hemisphere, Washington, DC (1976).
18. V. Gnielinski, Forced convection in ducts. In *Heat Exchanger Design Handbook*, Vol. 2, Chap. 2.5.1. Hemisphere, Washington, DC (1983).

EXPERIENCES SUR L'EBULLITION EN ECOULEMENT SOUS REFROIDI DANS UN CANAL ANNULAIRE VERTICAL

Résumé—Des expériences concernant le transfert thermique pendant l'ébullition en écoulement sous refroidi sont réalisées dans un canal vertical annulaire dont la paroi intérieure est chauffée et l'autre externe est isolée. Le fluide de travail est le R113. Les données expérimentales correspondent à trois débits-masse (579, 801 et 1102 kg $m^{-2} s^{-1}$), trois pressions (312, 277 et 243 kPa) et trois sous-refroidissements à l'entrée (20, 30 et 36,5°C). On identifie un phénomène multiple d'hystérésis. Les coefficients de transfert thermique pariétaux sont comparés aux prévisions de plusieurs formules et on suggère une amélioration de la formule de Shah pour les espaces annulaires.

EXPERIMENTE ZUM WÄRMEÜBERGANG BEI UNTERKÜHLTEM STRÖMUNGSSIEDEN IN EINEM VERTIKALEN RINGSPALT

Zusammenfassung—Experimente zum Wärmeübergang bei unterkühltem Strömungssieden werden in einem vertikalen Ringspalt, dessen Innenwand beheizt und Außenwand isoliert ist, durchgeführt. Das Arbeitsmittel ist R113. Es werden Ergebnisse für den Wärmeübergang bei drei Massenstromdichten (579; 801 und 1102 kg $m^{-2} s^{-1}$) drei Drücken (312; 277 und 243 kPa) und drei Eintrittsunterkühlungen (20,0; 30,0 und 36,5°C) mitgeteilt. Mehrfache Hysterese-Erscheinungen werden beobachtet. Die an der Wand gemessenen Wärmeübergangskoeffizienten werden mit Berechnungen nach verschiedenen Korrelationen verglichen; eine Verbesserung der Korrelation nach Shah für Ringspaltströmung wird vorgeschlagen.

ЭКСПЕРИМЕНТЫ ПО ТЕПЛООБМЕНУ ПРИ ТЕЧЕНИИ КИПЯЩЕЙ НЕДОГРЕТОЙ ЖИДКОСТИ В ВЕРТИКАЛЬНОМ КОЛЬЦЕВОМ КАНАЛЕ

Аннотация—Проведены эксперименты по теплообмену при течении кипящей недогретой жидкости в вертикальном кольцевом канале с нагретой внутренней и изолированной внешней стенками. Рабочей жидкостью являлся хладагент-113. Представлены данные по теплообмену в процессе течения кипящей жидкости при трех различных значениях массовой скорости (579, 801 и 1102 кг $м^{-2} с^{-1}$), давления (312, 277 и 243 кПа) и недогрева на входе (20,0; 30,0 и 36,5°C). Установлено явление множественного гистерезиса. Проведено сравнение экспериментальных значений коэффициента теплопереноса с расчетами по различным соотношениям, и предложен способ уточнения обобщенной зависимости Шаха для кольцевых каналов.